

ERROR ESTIMATION AND ADAPTIVITY FOR STOCHASTIC COLLOCATION FINITE ELEMENTS PART I: SINGLE-LEVEL APPROXIMATION

ALEX BESPALOV, DAVID J. SILVESTER, AND FENG XU

ABSTRACT. A general adaptive refinement strategy for solving linear elliptic partial differential equation with random data is proposed and analysed herein. The adaptive strategy extends the a posteriori error estimation framework introduced by Guignard & Nobile in 2018 (*SIAM J. Numer. Anal.*, **56**, 3121–3143) to cover problems with a *nonaffine* parametric coefficient dependence. A suboptimal, but nonetheless reliable and convenient implementation of the strategy involves approximation of the decoupled PDE problems with a common finite element approximation space. Computational results obtained using such a *single-level* strategy are presented in this paper (part I). Results obtained using a potentially more efficient *multilevel* approximation strategy, where meshes are individually tailored, will be discussed in part II of this work. The codes used to generate the numerical results are available [on GitHub](#).

1. INTRODUCTION

Partial differential equations (PDEs) with uncertain inputs feature prominently when modelling a host of physical phenomena and have become a de facto model over the last two decades, both in scientific computing and computational engineering. Sparse grid stochastic collocation representations of parametric uncertainty in combination with finite element discretization of physical space have become established as an alternative approach to Monte-Carlo strategies over the last decade, especially in the context of nonlinear PDE models or linear PDE problems that are nonlinear in the parameterisation of the uncertainty.

Sparse grid methods, where the set of sample points is adaptively generated, can be traced back to Gerstner & Griebel [17]. They have been extensively tested in a collocation setting; see for example, [11, 24]. A complementary concept that has shown a lot of promise is the employment of multilevel approaches that aim to reduce the computational cost through a hierarchy of spatial approximations; see for example, [20, 28]. In this contribution, we aim to combine these two complementary concepts in a rigorous manner with adaptivity driven by novel reliable a posteriori error estimates. Specifically, we will generalise and extend the adaptive framework proposed in the recent paper by Guignard & Nobile [18] and present a critical comparison of alternative strategies in the context of solving a representative model problem that combines strong anisotropy in the parametric dependence with singular behaviour in the physical space. We note that parametric adaptivity has also been explored in a Galerkin framework; see [5, 7, 9, 13, 14], and that

Date: August 23, 2022.

Acknowledgements. This work was supported by EPSRC grants EP/W010925/1, EP/P013317/1, and EP/P013791/1.

there are a number of recent papers aimed at proving dimension-independent convergence; see for example, [3, 6, 23, 29].

The convergence of a modified version of the adaptive algorithm in [18] has been established by Eigel et al. [12] and independently by Feischl & Scaglioni [16]. The authors of [16] note that the main obstacle in establishing convergence is “the interplay of parametric refinement and finite element refinement”. We focus on this interplay in this work. Specifically, after introducing the model problem in section 2 and setting up its discretization in section 3, we develop a general adaptive solution strategy in section 4. Computational results generated with adaptively refined *single-level* approximations (i.e., using the same spatial refinement for all collocation points) are discussed in section 5. A discussion of computational results obtained with a more efficient *multilevel* spatial refinement implementation of the adaptive algorithm in §4.3 is deferred to part II of this work.

2. A PARAMETRIC MODEL PROBLEM

Let $D \subset \mathbb{R}^2$ be a bounded Lipschitz domain with polygonal boundary ∂D . Let $\Gamma := \Gamma_1 \times \Gamma_2 \dots \times \Gamma_M$ denote the parameter domain in \mathbb{R}^M , where $M \in \mathbb{N}$ and each Γ_m ($m = 1, \dots, M$) is a bounded interval in \mathbb{R} . We introduce a probability measure $\pi(\mathbf{y}) := \prod_{m=1}^M \pi_m(y_m)$ on $(\Gamma, \mathcal{B}(\Gamma))$; here, π_m denotes a Borel probability measure on Γ_m ($m = 1, \dots, M$) and $\mathcal{B}(\Gamma)$ is the Borel σ -algebra on Γ .

We consider the following parametric elliptic problem: find $u : \overline{D} \times \Gamma \rightarrow \mathbb{R}$ satisfying

$$\begin{aligned} -\nabla \cdot (a(\cdot, \mathbf{y}) \nabla u(\cdot, \mathbf{y})) &= f \quad \text{in } D, \\ u(\cdot, \mathbf{y}) &= 0 \quad \text{on } \partial D \end{aligned} \tag{1}$$

π -almost everywhere on Γ (i.e., almost surely). Here, the deterministic right-hand side function $f \in L^2(D)$ and the coefficient a is a random field on $(\Gamma, \mathcal{B}(\Gamma), \pi)$ over $L^\infty(D)$. Furthermore, we assume that there exist constants a_{\min}, a_{\max} such that

$$0 < a_{\min} \leq \operatorname{ess\,inf}_{x \in D} a(x, \mathbf{y}) \leq \operatorname{ess\,sup}_{x \in D} a(x, \mathbf{y}) \leq a_{\max} < \infty \quad \pi\text{-a.e. on } \Gamma. \tag{2}$$

This assumption, in particular, implies the following norm equivalence: for any $v \in \mathbb{X} := H_0^1(D)$ there holds

$$a_{\min}^{1/2} \|\nabla v\|_{L^2(D)} \leq \|a^{1/2}(\cdot, \mathbf{y}) \nabla v\|_{L^2(D)} \leq a_{\max}^{1/2} \|\nabla v\|_{L^2(D)} \quad \pi\text{-a.e. on } \Gamma. \tag{3}$$

The parametric problem (1) is understood in the weak sense: given $f \in L^2(D)$, find $u : \Gamma \rightarrow \mathbb{X}$ such that

$$\int_D a(x, \mathbf{y}) \nabla u(x, \mathbf{y}) \cdot \nabla v(x) dx = \int_D f(x) v(x) dx \quad \forall v \in \mathbb{X}, \quad \pi\text{-a.e. on } \Gamma. \tag{4}$$

The above assumptions on a and f guarantee that the parametric problem (1) admits a unique weak solution u in the Bochner space $\mathbb{V} := L_\pi^p(\Gamma; \mathbb{X})$ for any $p \in [1, \infty]$; see [2, Lemma 1.1] for details.

3. MULTILEVEL STOCHASTIC COLLOCATION FINITE ELEMENT METHOD

For the numerical solution of problem (1) we propose to use the multilevel stochastic collocation finite element method (SC-FEM). We recall the main ideas and the construction of the approximation spaces in the following.

Let \mathcal{T}_\bullet be a mesh, i.e., a conforming triangulation of the spatial domain D into compact non-degenerate triangles $T \in \mathcal{T}_\bullet$ and denote by \mathcal{N}_\bullet the set of vertices of \mathcal{T}_\bullet . We restrict attention to the space of continuous piecewise linear finite elements for convenience,

$$\mathbb{X}_\bullet := \mathcal{S}_0^1(\mathcal{T}_\bullet) := \{v \in \mathbb{X} : v|_T \text{ is affine for all } T \in \mathcal{T}_\bullet\} \subset \mathbb{X} = H_0^1(D).$$

Recall that the standard basis of \mathbb{X}_\bullet is given by $\{\varphi_{\bullet,\xi} : \xi \in \mathcal{N}_\bullet \setminus \partial D\}$, where $\varphi_{\bullet,\xi}$ denotes the hat function associated with the vertex $\xi \in \mathcal{N}_\bullet$.

For mesh refinement, we employ newest vertex bisection (NVB); see, e.g., [27, 19]. We assume that any mesh \mathcal{T}_\bullet employed for the spatial discretization can be obtained by applying NVB refinement(s) to a given (coarse) initial mesh \mathcal{T}_0 .

For a given mesh \mathcal{T}_\bullet , let $\widehat{\mathcal{T}}_\bullet$ be the coarsest NVB refinement of \mathcal{T}_\bullet such that all edges of \mathcal{T}_\bullet have been bisected once (which corresponds to uniform refinement of all elements by three bisections). Then, $\widehat{\mathcal{N}}_\bullet$ denotes the set of vertices of $\widehat{\mathcal{T}}_\bullet$, and $\mathcal{N}_\bullet^+ := (\widehat{\mathcal{N}}_\bullet \setminus \mathcal{N}_\bullet) \setminus \partial D$ is the set of new interior vertices created by this refinement of \mathcal{T}_\bullet . The finite element space associated with $\widehat{\mathcal{T}}_\bullet$ is denoted by $\widehat{\mathbb{X}}_\bullet := \mathcal{S}_0^1(\widehat{\mathcal{T}}_\bullet)$, and $\{\widehat{\varphi}_{\bullet,\xi} : \xi \in \widehat{\mathcal{N}}_\bullet \setminus \partial D\}$ is the corresponding basis of hat functions. In §4, we will exploit the (H^1 -stable) decomposition

$$\widehat{\mathbb{X}}_\bullet = \mathbb{X}_\bullet \oplus \mathbb{Y}_\bullet, \quad \text{where } \mathbb{Y}_\bullet := \text{span}\{\widehat{\varphi}_{\bullet,\xi} : \xi \in \mathcal{N}_\bullet^+\}. \quad (5)$$

Note that $\mathbb{X}_\bullet \cap \mathbb{Y}_\bullet = \{0\}$, therefore the strengthened Cauchy–Schwarz inequality holds for the subspaces \mathbb{X}_\bullet and \mathbb{Y}_\bullet (see, e.g. [15]):

$$\exists \gamma \in [0, 1) \text{ such that } |(\nabla u, \nabla v)_{L^2(D)}| \leq \gamma \|\nabla u\|_{L^2(D)} \|\nabla v\|_{L^2(D)} \quad \forall u \in \mathbb{X}_\bullet, \forall v \in \mathbb{Y}_\bullet. \quad (6)$$

For a set of marked vertices $\mathcal{M}_\bullet \subseteq \mathcal{N}_\bullet^+$, let $\mathcal{T}_\circ := \text{refine}(\mathcal{T}_\bullet, \mathcal{M}_\bullet)$ be the coarsest NVB refinement of \mathcal{T}_\bullet such that $\mathcal{M}_\bullet \subset \mathcal{N}_\circ$, i.e., all marked vertices are vertices of \mathcal{T}_\circ .

For a fixed $\mathbf{z} \in \Gamma$, consider a mesh $\mathcal{T}_{\bullet,\mathbf{z}}$ and its uniform refinement $\widehat{\mathcal{T}}_{\bullet,\mathbf{z}}$ as well as the corresponding finite element spaces $\mathbb{X}_{\bullet,\mathbf{z}} := \mathcal{S}_0^1(\mathcal{T}_{\bullet,\mathbf{z}})$ and $\widehat{\mathbb{X}}_{\bullet,\mathbf{z}} := \mathcal{S}_0^1(\widehat{\mathcal{T}}_{\bullet,\mathbf{z}})$. We denote by $u_{\bullet,\mathbf{z}} \in \mathbb{X}_{\bullet,\mathbf{z}}$ the Galerkin finite element solution satisfying

$$\int_D a(x, \mathbf{z}) \nabla u_{\bullet,\mathbf{z}}(x) \cdot \nabla v(x) dx = \int_D f(x) v(x) dx \quad \forall v \in \mathbb{X}_{\bullet,\mathbf{z}}. \quad (7)$$

The enhanced Galerkin solution satisfying (7) for all $v \in \widehat{\mathbb{X}}_{\bullet,\mathbf{z}}$ is denoted by $\widehat{u}_{\bullet,\mathbf{z}} \in \widehat{\mathbb{X}}_{\bullet,\mathbf{z}}$.

Turning now to the parameter domain Γ , we consider a finite set \mathcal{Y}_\bullet of collocation points in Γ . The SC-FEM approximation of the solution u to parametric problem (1) is built as

$$u_\bullet^{\text{SC}} := \sum_{\mathbf{z} \in \mathcal{Y}_\bullet} u_{\bullet,\mathbf{z}}(x) L_{\bullet,\mathbf{z}}(\mathbf{y}), \quad (8)$$

where $u_{\bullet,\mathbf{z}} \in \mathbb{X}_{\bullet,\mathbf{z}}$ are Galerkin approximations satisfying (7) for $\mathbf{z} \in \mathcal{Y}_\bullet$, and $\{L_{\bullet,\mathbf{z}}(\mathbf{y}) = L_{\mathbf{z}}^{\mathcal{Y}_\bullet}(\mathbf{y}) : \mathbf{z} \in \mathcal{Y}_\bullet\}$ is a set of multivariable Lagrange basis functions associated with \mathcal{Y}_\bullet and satisfying $L_{\bullet,\mathbf{z}}(\mathbf{z}') = \delta_{\mathbf{z}\mathbf{z}'}$ for any $\mathbf{z}, \mathbf{z}' \in \mathcal{Y}_\bullet$. The total number of degrees of freedom in the SC-FEM approximations defined by (8) is given by $\sum_{\mathbf{z} \in \mathcal{Y}_\bullet} \dim(\mathbb{X}_{\bullet,\mathbf{z}})$. Note that the SC-FEM solution considered here follows the so-called *multilevel* construction (cf. [20, 16]) that allows $\mathbb{X}_{\bullet,\mathbf{z}} \neq \mathbb{X}_{\bullet,\mathbf{z}'}$ for $\mathbf{z} \neq \mathbf{z}'$. This is in contrast to the *single-level* SC-FEM approximations that employ the same finite element space \mathbb{X}_\bullet for all collocation points $\mathbf{z} \in \mathcal{Y}_\bullet$; see, e.g., [2, 25, 18].

Clearly, the choice of collocation points and the associated polynomial spaces on Γ is critical for efficient implementation of the generic SC-FEM construction outlined above,

particularly, for high-dimensional parametric problems. The established methodology here utilizes the sparse grid idea that goes back to Smoljak in [26] that is briefly described in the next section.

3.1. Sparse grid interpolation. To simplify the presentation we assume that $\Gamma_1 = \Gamma_2 = \dots = \Gamma_M \subset \mathbb{R}$. The methodology extends trivially to the general case. In order to construct a sparse grid $\mathcal{Y}_\bullet \subset \Gamma = \Gamma_1 \times \dots \times \Gamma_M$, one needs three ingredients:

- a family \mathcal{F} of *nested sets* of 1D nodes on Γ_m (one family for all $m = 1, \dots, M$); examples of such node sets are Leja points and Clenshaw–Curtis quadrature points;
- a strictly increasing function $\kappa : \mathbb{N}_0 \rightarrow \mathbb{N}_0$ associated with the chosen sets of 1D nodes and such that $\kappa(0) = 0$, $\kappa(1) = 1$ (e.g., $\kappa(i) = i$ for Leja points and $\kappa(i) = 2^{i-1} + 1$, $i > 1$, for Clenshaw–Curtis nodes with the usual doubling rule);
- a monotone (or, downward-closed) finite set $\Lambda_\bullet \subset \mathbb{N}^M$ of multi-indices, i.e., $\Lambda_\bullet = \{\boldsymbol{\nu} = (\nu_1, \dots, \nu_M) : \nu_m \in \mathbb{N}, \forall m = 1, \dots, M\}$ is such that $\#\Lambda_\bullet < \infty$ and

$$\boldsymbol{\nu} \in \Lambda_\bullet \implies \boldsymbol{\nu} - \boldsymbol{\varepsilon}_m \in \Lambda_\bullet \quad \forall m = 1, \dots, M \text{ such that } \nu_m > 1,$$

where $\boldsymbol{\varepsilon}_m$ denotes the m th unit multi-index, i.e., $(\boldsymbol{\varepsilon}_m)_i = \delta_{mi}$ for all $i = 1, \dots, M$. Note that any monotone index set Λ_\bullet contains the multi-index $\mathbf{1} = (1, 1, \dots, 1)$.

Now, for each $\boldsymbol{\nu} \in \Lambda_\bullet$, the set of collocation points along the m th coordinate axis in \mathbb{R}^M is given by the set $\mathcal{Y}_m^{\kappa(\nu_m)} \in \mathcal{F}$ of cardinality $\kappa(\nu_m)$ and we define

$$\mathcal{Y}^{(\boldsymbol{\nu})} := \mathcal{Y}_1^{\kappa(\nu_1)} \times \mathcal{Y}_2^{\kappa(\nu_2)} \times \dots \times \mathcal{Y}_M^{\kappa(\nu_M)}.$$

For a given index set Λ_\bullet , the *sparse grid* $\mathcal{Y}_\bullet = \mathcal{Y}_{\Lambda_\bullet}$ of collocation points on Γ is defined as

$$\mathcal{Y}_\bullet = \mathcal{Y}_{\Lambda_\bullet} := \bigcup_{\boldsymbol{\nu} \in \Lambda_\bullet} \mathcal{Y}^{(\boldsymbol{\nu})}.$$

Let \mathbb{P}_q denote the set of univariate polynomials of degree at most $q \in \mathbb{N}_0$. Given an index set Λ_\bullet , we define the polynomial space $\mathbb{P}_\bullet = \mathbb{P}_{\Lambda_\bullet}$ on Γ as

$$\mathbb{P}_\bullet = \mathbb{P}_{\Lambda_\bullet} := \bigoplus_{\boldsymbol{\nu} \in \Lambda_\bullet} \mathbb{P}_{\boldsymbol{\kappa}(\boldsymbol{\nu})-1} \text{ with } \mathbb{P}_{\boldsymbol{\kappa}(\boldsymbol{\nu})-1} := \bigotimes_{m=1}^M \mathbb{P}_{\kappa(\nu_m)-1} \text{ and } \boldsymbol{\kappa}(\boldsymbol{\nu}) := (\kappa(\nu_1), \dots, \kappa(\nu_M)).$$

We denote by $I_m^{\kappa(\nu_m)} : C^0(\Gamma_m; \mathbb{X}) \rightarrow \mathbb{P}_{\kappa(\nu_m)-1}(\Gamma_m; \mathbb{X})$ the univariate Lagrange interpolation operator associated with the set of nodes $\mathcal{Y}_m^{\kappa(\nu_m)} \subset \Gamma_m$. Setting $I_m^0 = 0$ for all $m = 1, \dots, M$, we define univariate detail operators

$$\Delta_m^{\kappa(\nu_m)} := I_m^{\kappa(\nu_m)} - I_m^{\kappa(\nu_m)-1}.$$

Now, the sparse grid collocation operator associated with the sparse grid $\mathcal{Y}_{\Lambda_\bullet}$ is defined as

$$S_\bullet = S_{\Lambda_\bullet} := \sum_{\boldsymbol{\nu} \in \Lambda_\bullet} \Delta^{\boldsymbol{\kappa}(\boldsymbol{\nu})}, \tag{9}$$

where $\Delta^{\boldsymbol{\kappa}(\boldsymbol{\nu})} := \bigotimes_{m=1}^M \Delta_m^{\kappa(\nu_m)}$ denotes the hierarchical surplus operator.

The operator S_{Λ_\bullet} can be written also as a linear combination of tensor products of univariate Lagrange interpolation operators as follows:

$$S_{\Lambda_\bullet} = \sum_{\boldsymbol{\nu} \in \Lambda_\bullet} c_{\boldsymbol{\nu}} \bigotimes_{m=1}^M I_m^{\kappa(\nu_m)} \quad \text{with} \quad c_{\boldsymbol{\nu}} := \sum_{\substack{\mathbf{j} \in \{0,1\}^M \\ (\boldsymbol{\nu} + \mathbf{j}) \in \Lambda_\bullet}} (-1)^{|\mathbf{j}|^1}. \quad (10)$$

This representation generates an efficient implementation of S_{Λ_\bullet} . Furthermore, the nestedness of univariate node sets and the monotonicity of the index set Λ_\bullet imply the interpolation property for the operator S_{Λ_\bullet} , i.e.,

$$S_{\Lambda_\bullet} : C^0(\Gamma; \mathbb{X}) \rightarrow \mathbb{P}_{\Lambda_\bullet}(\Gamma; \mathbb{X}) \quad \text{is such that} \quad S_{\Lambda_\bullet} v(\mathbf{z}) = v(\mathbf{z}) \quad \forall \mathbf{z} \in \mathcal{Y}_{\Lambda_\bullet}. \quad (11)$$

Therefore, the SC-FEM solution defined by (8) can be written as

$$u_\bullet^{\text{SC}}(x, \mathbf{y}) = S_\bullet U_\bullet(x, \mathbf{y}) = \sum_{\mathbf{z} \in \mathcal{Y}_\bullet} u_{\bullet\mathbf{z}}(x) L_{\bullet\mathbf{z}}(\mathbf{y}) \quad (12)$$

with a function $U_\bullet : \Gamma \rightarrow \mathcal{S}_0^1\left(\bigoplus_{\mathbf{z} \in \mathcal{Y}_\bullet} \mathcal{T}_{\bullet\mathbf{z}}\right)$ satisfying $U_\bullet(\mathbf{z}) = u_{\bullet\mathbf{z}}$ for all $\mathbf{z} \in \mathcal{Y}_\bullet$; here, $\bigoplus_{\mathbf{z} \in \mathcal{Y}_\bullet} \mathcal{T}_{\bullet\mathbf{z}}$ denotes the *overlay* of the meshes $\mathcal{T}_{\bullet\mathbf{z}}$, $\mathbf{z} \in \mathcal{Y}_\bullet$ (in other words, their coarsest common refinement).

The enhancement of the parametric component of the SC-FEM approximation given by (12) is done by enriching the index set Λ_\bullet (and, hence, expanding the set \mathcal{Y}_\bullet of collocation points). To that end, for a given index set Λ_\bullet , we introduce the margin

$$\mathbf{K}_\bullet = \mathbf{K}(\Lambda_\bullet) := \{\boldsymbol{\nu} \in \mathbb{N}^M \setminus \Lambda_\bullet : \boldsymbol{\nu} - \boldsymbol{\varepsilon}_m \in \Lambda_\bullet \text{ for some } m \in \{1, \dots, M\}\} \quad (13)$$

and the reduced margin

$$\mathbf{R}_\bullet = \mathbf{R}(\Lambda_\bullet) := \{\boldsymbol{\nu} \in \mathbf{K}(\Lambda_\bullet) : \boldsymbol{\nu} - \boldsymbol{\varepsilon}_m \in \Lambda_\bullet \text{ for all } m = 1, \dots, M \text{ such that } \nu_m > 1\}. \quad (14)$$

Note that for a monotone Λ_\bullet and for any subset of marked indices $\mathbf{M}_\bullet \subseteq \mathbf{R}_\bullet$, the index set $\Lambda_\bullet \cup \mathbf{M}_\bullet$ is also monotone.

4. HIERARCHICAL A POSTERIORI ERROR ESTIMATION AND ADAPTIVITY

In the sequel, we define $\|\cdot\|_{\mathbb{X}} := \|\nabla \cdot\|_{L^2(D)}$ and let $\|\cdot\|$ denote the norm in $\mathbb{V} = L_\pi^p(\Gamma, \mathbb{X})$ for a fixed $1 \leq p \leq \infty$. We will use a hierarchical construction (see, e.g., [1, Chapter 5]) to derive a reliable a posteriori estimate for the discretization error $u - u_\bullet^{\text{SC}} = u - S_\bullet U_\bullet \in \mathbb{V}$. To that end, we denote by $\hat{u}_\bullet^{\text{SC}}$ an enhanced SC-FEM approximation that reduces the discretization error, i.e.,

$$\|u - \hat{u}_\bullet^{\text{SC}}\| \leq q_{\text{sat}} \|u - u_\bullet^{\text{SC}}\| \quad (15)$$

with some constant $q_{\text{sat}} \in (0, 1)$ that is independent of discretization parameters. Then, by using the triangle inequality, we obtain

$$\|u - u_\bullet^{\text{SC}}\| \leq (1 - q_{\text{sat}})^{-1} \|\hat{u}_\bullet^{\text{SC}} - u_\bullet^{\text{SC}}\|. \quad (16)$$

We consider the following enhanced solution

$$\hat{u}_\bullet^{\text{SC}} := S_\bullet \hat{U}_\bullet + \left(\hat{S}_\bullet \tilde{U}_\bullet - S_\bullet U_\bullet \right), \quad (17)$$

where

$$\hat{U}_\bullet : \Gamma \rightarrow \mathcal{S}_0^1\left(\bigoplus_{\mathbf{z} \in \mathcal{Y}_\bullet} \hat{\mathcal{T}}_{\bullet\mathbf{z}}\right) \quad \text{is such that} \quad \hat{U}_\bullet(\mathbf{z}) = \hat{u}_{\bullet\mathbf{z}} \quad \forall \mathbf{z} \in \mathcal{Y}_\bullet, \quad (18)$$

$$\widehat{S}_\bullet = S_{\widehat{\Lambda}_\bullet} := \sum_{\nu \in \widehat{\Lambda}_\bullet} \Delta^{\kappa(\nu)}, \quad (19)$$

and

$$\widetilde{U}_\bullet : \Gamma \rightarrow \mathcal{S}_0^1 \left(\left[\bigoplus_{\mathbf{z} \in \widehat{\mathcal{Y}}_\bullet} \mathcal{T}_{\mathbf{z}} \right] \right) \text{ is defined so that } \widetilde{U}_\bullet(\mathbf{z}) = \widetilde{u}_{\bullet, \mathbf{z}} = \begin{cases} u_{\bullet, \mathbf{z}} & \forall \mathbf{z} \in \mathcal{Y}_\bullet, \\ u_{0\mathbf{z}} & \forall \mathbf{z} \in \widehat{\mathcal{Y}}_\bullet \setminus \mathcal{Y}_\bullet. \end{cases} \quad (20)$$

Here, to retain generality, $\widehat{\Lambda}_\bullet$ is any monotone index set that contains Λ_\bullet (e.g., $\widehat{\Lambda}_\bullet = \Lambda_\bullet \cup \mathbf{R}_\bullet$), and $\widehat{\mathcal{Y}}_\bullet$ is the set of collocation points generated by the index set $\widehat{\Lambda}_\bullet$.

A subtle feature of the construction (20) is the identification of $u_{0\mathbf{z}} \in \mathcal{S}_0^1(\mathcal{T}_{0\mathbf{z}})$ as the Galerkin approximation on a suitable (coarse) mesh $\mathcal{T}_{0\mathbf{z}}$ using the coefficient a sampled at a new collocation point $\mathbf{z} \in \widehat{\mathcal{Y}}_\bullet \setminus \mathcal{Y}_\bullet$. The construction of sample-specific meshes for new collocation points will be discussed in detail in part II of this work.

To summarise, the definition of $\widehat{u}_\bullet^{\text{SC}}$ in (17) is based on two enhanced (multilevel) SC-FEM approximations; namely,

- (i) $S_\bullet \widehat{U}_\bullet$ is determined by the same set \mathcal{Y}_\bullet of collocation points as the SC-FEM solution u_\bullet^{SC} but employs the enhanced Galerkin approximations $\widehat{u}_{\bullet, \mathbf{z}} \in \widehat{\mathbb{X}}_{\bullet, \mathbf{z}}$, and
- (ii) $\widehat{S}_\bullet \widetilde{U}_\bullet$ is determined by the same Galerkin approximations $u_{\bullet, \mathbf{z}} \in \mathbb{X}_{\bullet, \mathbf{z}}$ as u_\bullet^{SC} at each collocation point $\mathbf{z} \in \mathcal{Y}_\bullet$ in combination with (coarse) mesh Galerkin approximations $u_{0\mathbf{z}} \in \mathcal{S}_0^1(\mathcal{T}_{0\mathbf{z}})$ at all new collocation points $\mathbf{z} \in \widehat{\mathcal{Y}}_\bullet \setminus \mathcal{Y}_\bullet$. The term $(\widehat{S}_\bullet \widetilde{U}_\bullet - S_\bullet U_\bullet)$ in (17) is the hierarchical surplus associated with the enhanced approximation $\widehat{S}_\bullet \widetilde{U}_\bullet$.

Remark 1. An alternative construction of a function $\widehat{u}_\bullet^{\text{SC}}$ is given by

$$\widehat{u}_\bullet^{\text{SC}} := S_\bullet \widehat{U}_\bullet + \left(\widehat{S}_\bullet \widetilde{U}_{\bullet, 0} - S_\bullet U_{\bullet, 0} \right), \quad (21)$$

where \widehat{U}_\bullet and \widehat{S}_\bullet are defined as before by (18) and (19), respectively,

$$\widetilde{U}_{\bullet, 0} : \Gamma \rightarrow \mathcal{S}_0^1(\mathcal{T}_0) \text{ is such that } \widetilde{U}_{\bullet, 0}(\mathbf{z}') = u_{0\mathbf{z}'} \quad \forall \mathbf{z}' \in \widehat{\mathcal{Y}}_\bullet,$$

and

$$U_{\bullet, 0} : \Gamma \rightarrow \mathcal{S}_0^1(\mathcal{T}_0) \text{ is such that } U_{\bullet, 0}(\mathbf{z}) = u_{0\mathbf{z}} \quad \forall \mathbf{z} \in \mathcal{Y}_\bullet.$$

The advantage of this construction compared to that in (17) is in the ease of implementation of the parametric enhancement $\widehat{S}_\bullet \widetilde{U}_{\bullet, 0} - S_\bullet U_{\bullet, 0}$, as the involved Galerkin approximations $u_{0\mathbf{z}'}$ ($\mathbf{z}' \in \widehat{\mathcal{Y}}_\bullet$) and $u_{0\mathbf{z}}$ ($\mathbf{z} \in \mathcal{Y}_\bullet$) are all computed on the coarsest finite element mesh \mathcal{T}_0 .

We assume that $\widehat{u}_\bullet^{\text{SC}}$ defined by (17) satisfies the saturation property (15). Therefore, by using (12), (17) and the triangle inequality, we derive from (16)

$$\|u - u_\bullet^{\text{SC}}\| \leq \frac{1}{1 - q_{\text{sat}}} \left(\|S_\bullet(\widehat{U}_\bullet - U_\bullet)\| + \|\widehat{S}_\bullet \widetilde{U}_\bullet - S_\bullet U_\bullet\| \right). \quad (22)$$

The two norms on the right hand side of (22) can be seen as the spatial and the parametric components of an a posteriori estimate for the discretization error. We will denote these spatial and parametric error estimates as

$$\mu_\bullet := \|S_\bullet(\widehat{U}_\bullet - U_\bullet)\| \quad \text{and} \quad \tau_\bullet := \|\widehat{S}_\bullet \widetilde{U}_\bullet - S_\bullet U_\bullet\|, \quad (23)$$

respectively. The components of the error estimate are discussed in more detail below.

4.1. Spatial error estimate and spatial error indicators. For the spatial error estimate μ_\bullet , we can estimate component error contributions using the triangle inequality

$$\mu_\bullet = \|S_\bullet(\widehat{U}_\bullet - U_\bullet)\| \stackrel{(12)}{=} \left\| \sum_{\mathbf{z} \in \mathcal{Y}_\bullet} (\widehat{u}_{\bullet\mathbf{z}} - u_{\bullet\mathbf{z}}) L_{\bullet\mathbf{z}} \right\| \leq \sum_{\mathbf{z} \in \mathcal{Y}_\bullet} \|\widehat{u}_{\bullet\mathbf{z}} - u_{\bullet\mathbf{z}}\|_{\mathbb{X}} \|L_{\bullet\mathbf{z}}\|_{L^p_\pi(\Gamma)}. \quad (24)$$

The crude bound in (24) pinpoints the inbuilt advantage of stochastic Galerkin approximation over SC-FEM approximation in the context of solving elliptic PDEs with random data. Numerical experiments confirm that the componentwise bound gives nonrobust over-estimation of the error as the number of parameters is increased.

Despite the inaccuracy, we will demonstrate later that the componentwise bound can still be employed to define an error *indicator* that can be used to drive a reliable adaptive refinement process. While the norm $\|\widehat{u}_{\bullet\mathbf{z}} - u_{\bullet\mathbf{z}}\|_{\mathbb{X}}$ is computable, its evaluation for each $\mathbf{z} \in \mathcal{Y}_\bullet$ requires computation of the enhanced Galerkin approximation $\widehat{u}_{\bullet\mathbf{z}}$. It is computationally more efficient to *estimate* these error components using hierarchical error indicators. We review two possible approaches below.

Spatial hierarchical error indicator I. For each $\mathbf{z} \in \mathcal{Y}_\bullet$, we define $\mu_{\bullet\mathbf{z}} := \|e_{\bullet\mathbf{z}}\|_{\mathbb{X}}$, where $e_{\bullet\mathbf{z}} \in \mathbb{Y}_{\bullet\mathbf{z}}$ satisfies (recall that $\widehat{\mathbb{X}}_{\bullet\mathbf{z}} = \mathbb{X}_{\bullet\mathbf{z}} \oplus \mathbb{Y}_{\bullet\mathbf{z}}$)

$$\int_D \nabla e_{\bullet\mathbf{z}}(x) \cdot \nabla v(x) dx = \int_D f(x)v(x) dx - \int_D a(x, \mathbf{z}) \nabla u_{\bullet\mathbf{z}}(x) \cdot \nabla v(x) dx \quad \forall v \in \mathbb{Y}_{\bullet\mathbf{z}}. \quad (25)$$

Then, following the construction in [4] and using the norm equivalence in (3) the following estimate holds:

$$\|\widehat{u}_{\bullet\mathbf{z}} - u_{\bullet\mathbf{z}}\|_{\mathbb{X}} \leq a_{\min}^{-1} (1 - \gamma_{\mathbf{z}}^2)^{-1/2} \mu_{\bullet\mathbf{z}}, \quad (26)$$

where $\gamma_{\mathbf{z}} \in [0, 1)$ is the constant in the strengthened Cauchy–Schwarz inequality (6) for the subspaces $\mathbb{X}_{\bullet\mathbf{z}}, \mathbb{Y}_{\bullet\mathbf{z}}$. Moreover, from (24) we get the crude overestimate

$$\mu_\bullet = \|S_\bullet(\widehat{U}_\bullet - U_\bullet)\| \leq a_{\min}^{-1} (1 - \gamma^2)^{-1/2} \sum_{\mathbf{z} \in \mathcal{Y}_\bullet} \mu_{\bullet\mathbf{z}} \|L_{\bullet\mathbf{z}}\|_{L^p_\pi(\Gamma)}, \quad (27)$$

where $\gamma := \max\{\gamma_{\mathbf{z}} : \mathbf{z} \in \mathcal{Y}_\bullet\}$. Note that the constant a_{\min}^{-1} in (27) is the same as in [18].

Remark 2. *It is important that $\gamma_{\mathbf{z}}$ in (26) is independent of the coefficient sample $a(\cdot, \mathbf{z})$. Noting that γ only depends on the subspaces $\mathbb{X}_{\bullet\mathbf{z}}, \mathbb{Y}_{\bullet\mathbf{z}}$ and that all underlying triangulations are generated from the same coarse mesh \mathcal{T}_0 by applying NVB refinement(s), it is eminently plausible that there exists a uniform upper bound for γ for all nested sets of collocation points generated when running an adaptive algorithm. An alternative construction would include the coefficient sample $a(\cdot, \mathbf{z})$ in definition of the problem (25). If this was done then the constants $\tilde{\gamma}_{\mathbf{z}}$ would depend on the samples of the coefficient $a(\cdot, \mathbf{z})$ at collocation points in which case it is not so obvious that there exists a uniform upper bound for γ .*

While local error indicators are not explicitly defined in the above construction, they can be easily derived from the computed error estimator $e_{\bullet\mathbf{z}}$. For example, for each element $T \in \mathcal{T}_{\bullet\mathbf{z}}$, the (spatial) error indicator associated with T is given by

$$\mu_{\bullet\mathbf{z}}(T) := \|e_{\bullet\mathbf{z}}|_T\|_{\mathbb{X}}.$$

Alternatively, the (spatial) error indicators $\mu_{\bullet\mathbf{z}}(\xi)$ associated with interior edge midpoints $\xi \in \mathcal{N}_{\bullet\mathbf{z}}^+$ are given by components of the solution vector to the linear system stemming from the discrete formulation (25).

Spatial hierarchical error indicator II. Recall that $\mathbb{Y}_{\bullet\mathbf{z}} := \text{span}\{\widehat{\varphi}_{\bullet\mathbf{z},\xi} : \xi \in \mathcal{N}_{\bullet\mathbf{z}}^+\}$ (see (5)). For each $\mathbf{z} \in \mathcal{Y}_{\bullet}$, we can define the two-level error indicators associated with interior edge midpoints:

$$\mu_{\bullet\mathbf{z}}(\xi) := \frac{|(f, \widehat{\varphi}_{\bullet\mathbf{z},\xi})_{L^2(D)} - (a(\cdot, \mathbf{z}) \nabla u_{\bullet\mathbf{z}}, \nabla \widehat{\varphi}_{\bullet\mathbf{z},\xi})_{L^2(D)}|}{\|\widehat{\varphi}_{\bullet\mathbf{z},\xi}\|_{\mathbb{X}}} \quad \text{for all } \xi \in \mathcal{N}_{\bullet\mathbf{z}}^+. \quad (28)$$

These indicators can then be combined to produce the two-level indicator

$$\mu_{\bullet\mathbf{z}}^2 := \sum_{\xi \in \mathcal{N}_{\bullet\mathbf{z}}^+} \mu_{\bullet\mathbf{z}}^2(\xi) \quad (29)$$

that satisfies (see [22, 21])

$$\|a^{1/2}(\cdot, \mathbf{z}) \nabla (\widehat{u}_{\bullet\mathbf{z}} - u_{\bullet\mathbf{z}})\|_{L^2(D)} \leq a_{\min}^{-1/2} C_{\text{est}} \mu_{\bullet\mathbf{z}}, \quad (30)$$

where a_{\min} is the constant in (3) and C_{est} is a generic constant that only depends on the coarse mesh \mathcal{T}_0 .

Using again the norm equivalence in (3), we get the following estimate of the error:

$$\begin{aligned} \mu_{\bullet} &= \|S_{\bullet}(\widehat{U}_{\bullet} - U_{\bullet})\| \leq a_{\min}^{-1/2} \sum_{\mathbf{z} \in \mathcal{Y}_{\bullet}} \|a^{1/2}(\cdot, \mathbf{z}) \nabla (\widehat{u}_{\bullet\mathbf{z}} - u_{\bullet\mathbf{z}})\|_{L^2(D)} \|L_{\bullet\mathbf{z}}\|_{L_{\pi}^p(\Gamma)} \\ &\leq a_{\min}^{-1} C_{\text{est}} \sum_{\mathbf{z} \in \mathcal{Y}_{\bullet}} \mu_{\bullet\mathbf{z}} \|L_{\bullet\mathbf{z}}\|_{L_{\pi}^p(\Gamma)}. \end{aligned} \quad (31)$$

The advantage of hierarchical error estimators over the residual estimators discussed by Guignard & Nobile in [18] is that they provide information about potential error reduction associated with local refinement in space or with enhancement of the parametric approximation, see [5, 9]. They also provide a more natural starting point for a rigorous convergence analysis of adaptive strategies, see [6].

4.2. Parametric error estimate and parametric error indicators. We now focus on the parametric error estimate τ_{\bullet} in (23). First, recalling the definitions of the operators S_{\bullet} and \widehat{S}_{\bullet} in (9) and (19), respectively, we find that

$$\begin{aligned} \widehat{S}_{\bullet} \widetilde{U}_{\bullet} - S_{\bullet} U_{\bullet} &= \sum_{\nu \in \widehat{\Lambda}_{\bullet}} \Delta^{\kappa(\nu)} \widetilde{U}_{\bullet} - \sum_{\nu \in \Lambda_{\bullet}} \Delta^{\kappa(\nu)} U_{\bullet} = \\ &= \sum_{\nu \in \Lambda_{\bullet}} \Delta^{\kappa(\nu)} (\widetilde{U}_{\bullet} - U_{\bullet}) + \sum_{\nu \in \widehat{\Lambda}_{\bullet} \setminus \Lambda_{\bullet}} \Delta^{\kappa(\nu)} \widetilde{U}_{\bullet} \stackrel{(20)}{=} \sum_{\nu \in \widehat{\Lambda}_{\bullet} \setminus \Lambda_{\bullet}} \Delta^{\kappa(\nu)} \widetilde{U}_{\bullet}. \end{aligned} \quad (32)$$

On the other hand, thanks to Λ_{\bullet} and $\widehat{\Lambda}_{\bullet}$ being monotone, we can write

$$\begin{aligned} (\widehat{S}_{\bullet} \widetilde{U}_{\bullet} - S_{\bullet} U_{\bullet})(x, \mathbf{y}) &= \sum_{\mathbf{z} \in \widehat{\mathcal{Y}}_{\bullet}} \widetilde{u}_{\bullet\mathbf{z}}(x) \widehat{L}_{\bullet\mathbf{z}}(\mathbf{y}) - \sum_{\mathbf{z} \in \mathcal{Y}_{\bullet}} u_{\bullet\mathbf{z}}(x) L_{\bullet\mathbf{z}}(\mathbf{y}) \\ &\stackrel{(20)}{=} \sum_{\mathbf{z} \in \mathcal{Y}_{\bullet}} u_{\bullet\mathbf{z}}(x) (\widehat{L}_{\bullet\mathbf{z}}(\mathbf{y}) - L_{\bullet\mathbf{z}}(\mathbf{y})) + \sum_{\mathbf{z} \in \widehat{\mathcal{Y}}_{\bullet} \setminus \mathcal{Y}_{\bullet}} u_{0\mathbf{z}}(x) \widehat{L}_{\bullet\mathbf{z}}(\mathbf{y}), \end{aligned}$$

where $\widehat{L}_{\bullet, \mathbf{z}}(\mathbf{y}) = L_{\mathbf{z}}^{\widehat{\mathcal{Y}}_{\bullet}}(\mathbf{y})$ denotes the Lagrange polynomial basis function associated with the point $\mathbf{z} \in \widehat{\mathcal{Y}}_{\bullet}$ and satisfying $\widehat{L}_{\bullet, \mathbf{z}}(\mathbf{z}') = \delta_{\mathbf{z}\mathbf{z}'}$ for any $\mathbf{z}, \mathbf{z}' \in \widehat{\mathcal{Y}}_{\bullet}$. Note that for any $\mathbf{z}' \in \widehat{\mathcal{Y}}_{\bullet}$ there holds

$$\begin{aligned} (\widehat{S}_{\bullet} \widetilde{U}_{\bullet} - S_{\bullet} U_{\bullet})(x, \mathbf{z}') &= \begin{cases} \sum_{\mathbf{z} \in \mathcal{Y}_{\bullet}} u_{\bullet, \mathbf{z}}(x) (\delta_{\mathbf{z}\mathbf{z}'} - \delta_{\mathbf{z}\mathbf{z}'}') + \sum_{\mathbf{z} \in \widehat{\mathcal{Y}}_{\bullet} \setminus \mathcal{Y}_{\bullet}} u_{0\mathbf{z}}(x) \delta_{\mathbf{z}\mathbf{z}'} & \text{if } \mathbf{z}' \in \mathcal{Y}_{\bullet}, \\ \sum_{\mathbf{z} \in \mathcal{Y}_{\bullet}} u_{\bullet, \mathbf{z}}(x) (\delta_{\mathbf{z}\mathbf{z}'} - L_{\bullet, \mathbf{z}}(\mathbf{z}')) + \sum_{\mathbf{z} \in \widehat{\mathcal{Y}}_{\bullet} \setminus \mathcal{Y}_{\bullet}} u_{0\mathbf{z}}(x) \delta_{\mathbf{z}\mathbf{z}'} & \text{if } \mathbf{z}' \in \widehat{\mathcal{Y}}_{\bullet} \setminus \mathcal{Y}_{\bullet}. \end{cases} \\ &= \begin{cases} 0 & \text{if } \mathbf{z}' \in \mathcal{Y}_{\bullet}, \\ -u_{\bullet}^{\text{SC}}(x, \mathbf{z}') + u_{0\mathbf{z}'}(x) & \text{if } \mathbf{z}' \in \widehat{\mathcal{Y}}_{\bullet} \setminus \mathcal{Y}_{\bullet}. \end{cases} \end{aligned}$$

Therefore,

$$\tau_{\bullet} = \|\widehat{S}_{\bullet} \widetilde{U}_{\bullet} - S_{\bullet} U_{\bullet}\| = \left\| \sum_{\mathbf{z} \in \widehat{\mathcal{Y}}_{\bullet} \setminus \mathcal{Y}_{\bullet}} (u_{0\mathbf{z}} - u_{\bullet}^{\text{SC}}(\cdot, \mathbf{z})) \widehat{L}_{\bullet, \mathbf{z}} \right\|. \quad (33)$$

The parametric estimate τ_{\bullet} is thus computable; calculating it requires extra PDE solves on coarse meshes $\mathcal{T}_{0\mathbf{z}}$ for a small number of collocation points $\mathbf{z} \in \widehat{\mathcal{Y}}_{\bullet} \setminus \mathcal{Y}_{\bullet}$.

The natural parametric error indicators associated with (32) are given by

$$\tau_{\bullet, \nu} := \|\Delta^{\kappa(\nu)} \widetilde{U}_{\bullet}\|, \quad \nu \in \widehat{\Lambda}_{\bullet} \setminus \Lambda_{\bullet}. \quad (34)$$

Remark 3. If the enriched index set $\widehat{\Lambda}_{\bullet}$ is obtained using the reduced margin of Λ_{\bullet} , i.e., $\widehat{\Lambda}_{\bullet} \setminus \Lambda_{\bullet} = \text{R}(\Lambda_{\bullet})$, then the collocation points in the set $\widehat{\mathcal{Y}}_{\bullet} \setminus \mathcal{Y}_{\bullet}$ can be grouped together according to the ‘generating’ multi-index $\nu \in \widehat{\Lambda}_{\bullet} \setminus \Lambda_{\bullet}$ such that

$$\widehat{\mathcal{Y}}_{\bullet} \setminus \mathcal{Y}_{\bullet} = \bigcup_{\nu \in \widehat{\Lambda}_{\bullet} \setminus \Lambda_{\bullet}} \widetilde{\mathcal{Y}}_{\bullet, \nu} \quad \text{and} \quad \widetilde{\mathcal{Y}}_{\bullet, \nu} \cap \widetilde{\mathcal{Y}}_{\bullet, \nu'} = \emptyset \quad \forall \nu, \nu' \in \widehat{\Lambda}_{\bullet} \setminus \Lambda_{\bullet}, \nu \neq \nu'.$$

In this case, we conclude from (32) and (33) that

$$\tau_{\bullet} = \|\widehat{S}_{\bullet} \widetilde{U}_{\bullet} - S_{\bullet} U_{\bullet}\| = \left\| \sum_{\nu \in \widehat{\Lambda}_{\bullet} \setminus \Lambda_{\bullet}} \sum_{\mathbf{z} \in \widetilde{\mathcal{Y}}_{\bullet, \nu}} (u_{0\mathbf{z}} - u_{\bullet}^{\text{SC}}(\cdot, \mathbf{z})) \widehat{L}_{\bullet, \mathbf{z}} \right\|,$$

and the associated parametric error indicators are given by

$$\widetilde{\tau}_{\bullet, \nu} = \sum_{\mathbf{z} \in \widetilde{\mathcal{Y}}_{\bullet, \nu}} \|u_{0\mathbf{z}} - u_{\bullet}^{\text{SC}}(\cdot, \mathbf{z})\|_{\mathbb{X}} \|\widehat{L}_{\bullet, \mathbf{z}}\|_{L_{\pi}^p(\Gamma)}, \quad \nu \in \widehat{\Lambda}_{\bullet} \setminus \Lambda_{\bullet}. \quad (35)$$

Note that for linearly growing sets of Leja points, one has $\tau_{\bullet, \nu} = \widetilde{\tau}_{\bullet, \nu}$, since for each $\nu \in \widehat{\Lambda}_{\bullet} \setminus \Lambda_{\bullet}$, the set $\widetilde{\mathcal{Y}}_{\bullet, \nu}$ consists of a single point $\mathbf{z}_{\nu} \in \widehat{\mathcal{Y}}_{\bullet} \setminus \mathcal{Y}_{\bullet}$.

Remark 4. All the arguments in this section extend trivially to the parametric error estimate and parametric error indicators derived from the alternative construction (21) of the enhanced SC-FEM solution $\widehat{u}_{\bullet}^{\text{SC}}$.

4.3. Adaptivity. A general multilevel SC-FEM adaptive algorithm is presented below. There are two features worth noting at the outset. First, the refinement of finite element approximations and the enrichment of the set of collocation points are driven by the error indicators $\mu_{\bullet, \mathbf{z}}$ and $\tau_{\bullet, \nu}$ discussed above. Second, the error estimates μ_{\bullet} and τ_{\bullet} in (23) only need to be calculated periodically; their combination is required for reliable termination of the adaptive process and to provide reassurance that the SC-FEM error is decreasing at an acceptable rate.

Algorithm 5. Input: $\Lambda_0 = \{1\}$; $\mathcal{T}_{0\mathbf{z}}$ for all $\mathbf{z} \in \widehat{\mathcal{Y}}_0 := \mathcal{Y}_{\Lambda_0 \cup \text{R}(\Lambda_0)}$; marking criterion. Set the iteration counter $\ell := 0$, the output counter k and the error tolerance.

- (i) Compute Galerkin approximations $\{u_{\ell\mathbf{z}} \in \mathbb{X}_{\ell\mathbf{z}} : \mathbf{z} \in \widehat{\mathcal{Y}}_\ell\}$ by solving (7).
- (ii) Compute the spatial error indicators $\{\mu_{\ell\mathbf{z}} : \mathbf{z} \in \mathcal{Y}_\ell\}$ by solving (25) (or the indicators $\{\mu_{\ell\mathbf{z}}(\xi) : \mathbf{z} \in \mathcal{Y}_\ell, \xi \in \mathcal{N}_{\ell\mathbf{z}}^+\}$ given by (28)).
- (iii) Compute the parametric error indicators $\{\tau_{\ell\nu} : \nu \in \widehat{\Lambda}_\ell \setminus \Lambda_\ell\}$ given by (34) (or the indicators $\{\tilde{\tau}_{\ell\nu} : \nu \in \widehat{\Lambda}_\ell \setminus \Lambda_\ell\}$ given by (35)).
- (iv) Use a marking criterion to determine $\mathcal{M}_{\ell\mathbf{z}} \subseteq \mathcal{N}_{\ell\mathbf{z}}^+$ for all $\mathbf{z} \in \mathcal{Y}_\ell$ and $\Upsilon_\ell \subseteq \widehat{\Lambda}_\ell \setminus \Lambda_\ell$.
- (v) For all $\mathbf{z} \in \mathcal{Y}_\ell$, set $\mathcal{T}_{(\ell+1)\mathbf{z}} := \text{refine}(\mathcal{T}_{\ell\mathbf{z}}, \mathcal{M}_{\ell\mathbf{z}})$.
- (vi) Set $\Lambda_{\ell+1} := \Lambda_\ell \cup \Upsilon_\ell$, $\widehat{\mathcal{Y}}_{\ell+1} := \mathcal{Y}_{\Lambda_{\ell+1} \cup \text{R}(\Lambda_{\ell+1})}$, and construct $\mathcal{T}_{(\ell+1)\mathbf{z}} := \mathcal{T}_{0\mathbf{z}}$ for all $\mathbf{z} \in \widehat{\mathcal{Y}}_{\ell+1} \setminus \mathcal{Y}_\ell$.
- (vii) If $\ell = jk, j \in \mathbb{N}$, compute the spatial and parametric error estimates μ_ℓ and τ_ℓ and exit if $\mu_\ell + \tau_\ell < \text{errortolerance}$.
- (viii) Increase the counter $\ell \mapsto \ell + 1$ and goto (i).

Output: For some specific $\ell_* = jk \in \mathbb{N}$, the algorithm returns the multilevel SC-FEM approximation $u_{\ell_*}^{\text{SC}}$ computed via (8) from Galerkin approximations $\{u_{\ell_*\mathbf{z}} \in \mathbb{X}_{\ell_*\mathbf{z}} : \mathbf{z} \in \mathcal{Y}_{\ell_*}\}$ together with a corresponding error estimate $\mu_{\ell_*} + \tau_{\ell_*}$.

A simple marking strategy for step (iv) of Algorithm 5 is specified next.

Marking criterion. Input: error reduction indicators $\{\mu_{\ell\mathbf{z}}(\xi) : \mathbf{z} \in \mathcal{Y}_\ell, \xi \in \mathcal{N}_{\ell\mathbf{z}}^+\}$, $\{\mu_{\ell\mathbf{z}} = (\sum_{\xi \in \mathcal{N}_{\ell\mathbf{z}}^+} \mu_{\ell\mathbf{z}}^2(\xi))^{1/2} : \mathbf{z} \in \mathcal{Y}_\ell\}$, and $\{\tau_{\ell\nu} : \nu \in \widehat{\Lambda}_\ell \setminus \Lambda_\ell\}$; marking parameters $0 < \theta_{\mathbb{X}}, \theta_{\mathbb{Y}} \leq 1$ and $\vartheta > 0$.

- If $\sum_{\mathbf{z} \in \mathcal{Y}_\ell} \mu_{\ell\mathbf{z}} \|L_{\ell\mathbf{z}}\|_{L_\pi^p(\Gamma)} \geq \vartheta \sum_{\nu \in \widehat{\Lambda}_\ell \setminus \Lambda_\ell} \tau_{\ell\nu}$, then proceed as follows:
 - set $\Upsilon_\ell := \emptyset$
 - for each $\mathbf{z} \in \mathcal{Y}_\ell$, determine $\mathcal{M}_{\ell\mathbf{z}} \subseteq \mathcal{N}_{\ell\mathbf{z}}^+$ of minimal cardinality such that

$$\theta_{\mathbb{X}} \mu_{\ell\mathbf{z}}^2 \leq \sum_{\xi \in \mathcal{M}_{\ell\mathbf{z}}} \mu_{\ell\mathbf{z}}^2(\xi). \quad (36)$$

- Otherwise, if $\sum_{\mathbf{z} \in \mathcal{Y}_\ell} \mu_{\ell\mathbf{z}} \|L_{\ell\mathbf{z}}\|_{L_\pi^p(\Gamma)} < \vartheta \sum_{\nu \in \widehat{\Lambda}_\ell \setminus \Lambda_\ell} \tau_{\ell\nu}$, then proceed as follows:
 - set $\mathcal{M}_{\ell\mathbf{z}} := \emptyset$ for all $\mathbf{z} \in \mathcal{Y}_\ell$
 - determine $\Upsilon_\ell \subseteq \widehat{\Lambda}_\ell \setminus \Lambda_\ell$ of minimal cardinality such that

$$\theta_{\mathbb{Y}} \sum_{\nu \in \widehat{\Lambda}_\ell \setminus \Lambda_\ell} \tau_{\ell\nu} \leq \sum_{\nu \in \Upsilon_\ell} \tau_{\ell\nu}. \quad (37)$$

Output: $\mathcal{M}_{\ell\mathbf{z}} \subseteq \mathcal{N}_{\ell\mathbf{z}}^+$ for all $\mathbf{z} \in \mathcal{Y}_\ell$ and $\Upsilon_\ell \subseteq \widehat{\Lambda}_\ell \setminus \Lambda_\ell$.

The rationale for checking convergence periodically in Algorithm 5 (rather than every iteration) is that direct computation of the spatial and parametric error estimates in (23) incurs a significant computational overhead. In particular, the calculation of the spatial error estimate μ_ℓ requires the solution of the PDE on uniform refinements of all meshes associated with collocation points generated by the current index set.

We set $p = 2$ when computing the norms in $\mathbb{V} = L_\pi^p(\Gamma, \mathbb{X})$ in practice. The only other detail needed to implement Algorithm 5 is the specification of the starting meshes $\mathcal{T}_{0\mathbf{z}}$ when introducing new collocation points¹ in step (vi). This specification will be shown to be crucially important in part II of this work. In the standard *single-level* SC-FEM setting discussed below, the same current mesh \mathcal{T}_\bullet is assigned to all new collocation points added in step (vi) of Algorithm 5. Accordingly, the meshes $\mathcal{T}_{0\mathbf{z}}$ ($\mathbf{z} \in \hat{\mathcal{Y}}_\bullet \setminus \mathcal{Y}_\bullet$) are set to be identical to the meshes $\mathcal{T}_{\bullet\mathbf{z}} = \mathcal{T}_\bullet$ ($\mathbf{z} \in \mathcal{Y}_\bullet$). Thus, the construction of an overlay mesh when computing $\tilde{u}_{\bullet\mathbf{z}}$ in (20) is not needed in the single-level setting.

5. NUMERICAL EXPERIMENTS

The numerical results presented in this section show that adaptive SC-FEM strategies are competitive in terms of computational effort with single-level adaptive stochastic Galerkin (SG) approximation—certainly in the context of the model problem that is the focus of this study. The results also provide a basis for comparison with multilevel adaptive SC-FEM in part II.

The single-level refinement strategy that will be employed is the obvious and natural simplification of the multilevel strategy described in §4.3. Thus, at each step ℓ of the process, we compute the error indicators associated with the SC-FEM solution $u_{\ell\mathbf{z}}$ (steps (ii)–(iii) of Algorithm 5). Specifically, we employ the spatial hierarchical error indicator \mathbf{I} computed by solving (25) and the parametric error indicators given by (34). The marking criterion listed in §4.3 (we set $\vartheta = 1$) then identifies the refinement type by comparing the (global) spatial error estimate $\bar{\mu}_\ell := \|\mu_{\ell\mathbf{z}}\|_{L_{\ell\mathbf{z}}\|_{L_\pi^p(\Gamma)}\|_{\ell_1}$ with the parametric error estimate $\bar{\tau}_\ell := \|\tau_{\ell\mathbf{z}}\|_{\ell_1}$. Thus, if $\bar{\mu}_\ell$ is less than $\bar{\tau}_\ell$ then we enforce a parametric refinement: choosing a bigger index set but keeping the finite element space unchanged; otherwise, we effect a spatial refinement: choosing an enhanced finite element space but keeping the index set unchanged. The marking strategy also generates the refinement process with the qualification that to effect a spatial refinement, we use Dörfler marking with marking threshold $\theta_\mathbb{X}$ to produce sets of marked elements from the (single) mesh \mathcal{T}_ℓ . A refined triangulation $\mathcal{T}_{\ell+1}$ can then be constructed by refining the elements in the *union* of these individual sets $\mathcal{M}_{\ell\mathbf{z}}$ ($\mathbf{z} \in \mathcal{Y}_\ell$) of marked elements.

5.1. Test case I: affine coefficient data. We set $f = 1$ and look to solve the model problem on the square-shaped domain $D = (0, 1)^2$ with random field coefficient given by

$$a(x, \mathbf{y}) = a_0(x) + \sum_{m=1}^M a_m(x) y_m, \quad x \in D, \mathbf{y} \in \Gamma. \quad (38)$$

The specific problem we consider is taken from [9]. The parameters y_m in (38) are the images of uniformly distributed independent mean-zero random variables, so that $\pi_m = \pi_m(y_m)$ is the associated probability measure on $\Gamma_m = [-1, 1]$. The expansion coefficients

¹Starting meshes also need to be specified in the initialization phase.

$a_m, m \in \mathbb{N}_0$ are chosen to represent planar Fourier modes of increasing total order. Thus, we fix $a_0(x) := 1$ and set

$$a_m(x) := \alpha_m \cos(2\pi\beta_1(m)x_1) \cos(2\pi\beta_2(m)x_2), \quad x = (x_1, x_2) \in (0, 1) \times (0, 1). \quad (39)$$

The modes are ordered so that for any $m \in \mathbb{N}$,

$$\beta_1(m) = m - k(m)(k(m) + 1)/2 \quad \text{and} \quad \beta_2(m) = k(m) - \beta_1(m) \quad (40)$$

with $k(m) = \lfloor -1/2 + \sqrt{1/4 + 2m} \rfloor$ and the amplitude coefficients are constructed so that $\alpha_m = \bar{\alpha}m^{-2}$ with $\bar{\alpha} = 0.547$. (This is referred to as the *slow decay case* in [9].) The precise definition of the amplitude coefficients ensures that the requirement (2) is valid so the test problem is well posed in the sense discussed in section 2.

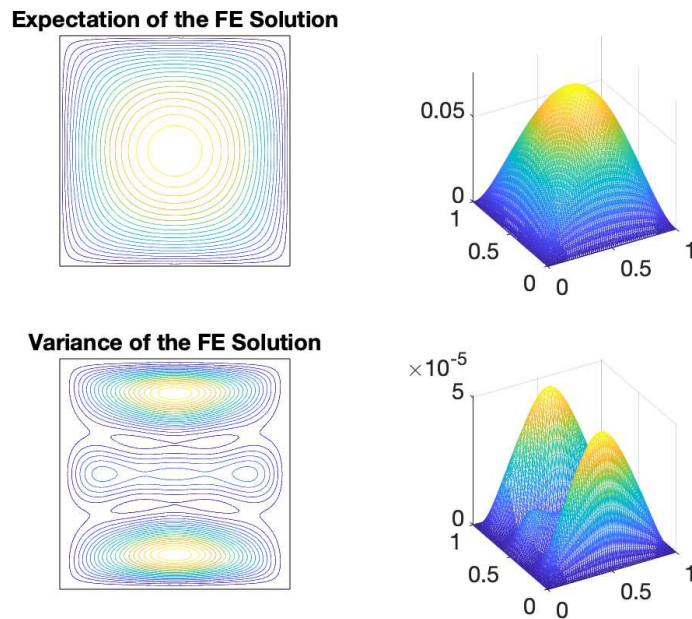


FIGURE 1. Reference solution for test case I.

A reference solution to this problem is illustrated in Fig. 1. This solution was generated by running the adaptive algorithm with M set to 4, the marking parameters θ_x and θ_y both set to 0.3 and with `errortolerance` set to `6e-3`. This tolerance was satisfied after 20 spatial refinement steps and 5 parametric refinement steps (25 iterations in total).

The plots in Fig. 2 show the initial mesh and the mesh when the error tolerance is reached. The final mesh can be seen to be locally refined to resolve weak singularities in the corners. The number of vertices in the final mesh (that is, the dimension of the linear system that is solved at every collocation point) is **16,473**.

The parametric approximation initially consists of a single collocation point. There were 13 Clenshaw–Curtis sparse grid collocation points when the error tolerance is reached. The corresponding highly anisotropic sparse grid indices are listed in Table 1. We note that the resolution is concentrated in the first three coordinates and that there is no refinement in the coordinates corresponding to the fourth mode in the expansion (38). (The fourth mode would be activated if we were to run with a slightly tighter tolerance, say `3e-3`.)

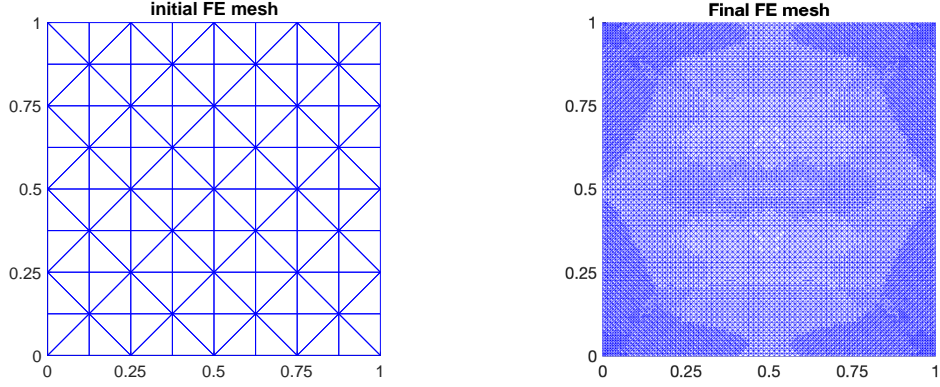


FIGURE 2. The initial mesh (left) and final mesh (right) generated by the single-level adaptive SC-FEM strategy for test case I with error tolerance set to $6\text{e-}3$.

TABLE 1. Anisotropic approximation comparison for test case I.

sparse grid indices	parametric approximation space for SG
1 1 1 1	0 0 0 0
2 1 1 1	1 0 0 0
3 1 1 1	2 0 0 0
4 1 1 1	3 0 0 0
5 1 1 1	4 0 0 0
1 2 1 1	0 1 0 0
2 2 1 1	1 1 0 0
3 2 1 1	2 1 0 0
1 3 1 1	0 2 0 0
2 3 1 1	1 0 0 1 0
3 3 1 1	1 0 1 0 0
1 1 2 1	0 0 1 0 0
1 1 3 1	2 0 1 0 0
	3 1 0 0 0
	0 0 0 1 0
	0 0 0 0 1

The evolution of the component error estimates and the global error indicators is reported in Fig. 3. The key point here is that the nature of the refinement step (parametric or spatial) is determined by the relative size of the component global *error indicators* (shown in the bottom plot). Thus it is reassuring to see the associated parametric and spatial error estimates (top plot) decrease monotonically after the first few steps. Note that if the saturation assumption (15) is uniformly satisfied then the combined error estimate $\eta_\ell := \mu_\ell + \tau_\ell$ is guaranteed to decrease at every step. In contrast, the total error indicator $\bar{\eta}_\ell := \bar{\mu}_\ell + \bar{\tau}_\ell$ can be seen to *increase* at iteration steps that follow a parametric refinement. The fact that the rate of the estimated error reduction in the bottom plot is much slower than the rate of error reduction in the top plot clearly shows the necessity of computing η_ℓ periodically in Algorithm 5.

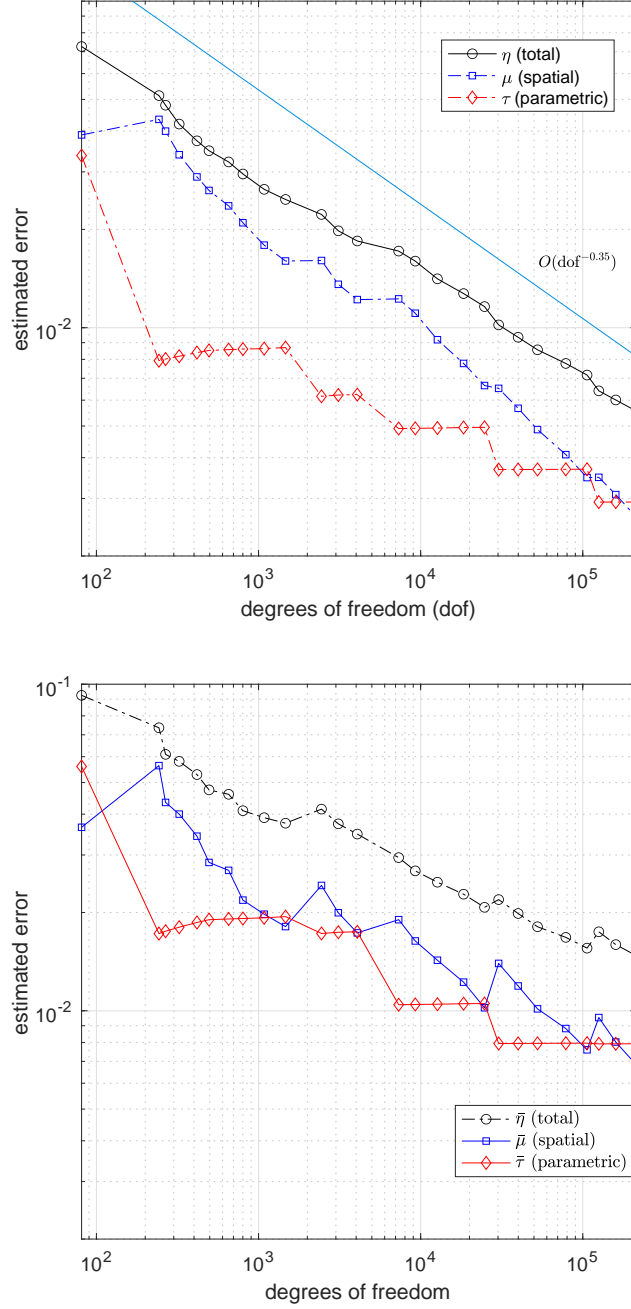


FIGURE 3. Evolution of the error estimates (top) and the error reduction indicators (bottom) generated by the single-level SC-FEM adaptive strategy for test case I with error tolerance set to $6\text{e-}3$.

To check the robustness of the SC error estimation strategy we can compare the pattern of refinement with the pattern that results when the same test problem (with $M = \infty$) is solved using the single-level stochastic Galerkin adaptive strategy in [7, 6] that is built into T-IFISS [8](with a slightly smaller accuracy tolerance). When we ran this test, the numerical solution generated by SG is visually identical to that reference solution in

Fig. 1 with agreement to 4 decimal digits in the maximum value of the mean (0.07582 vs 0.07581) as well as the maximum value of the standard deviation (0.00710 vs 0.00709).

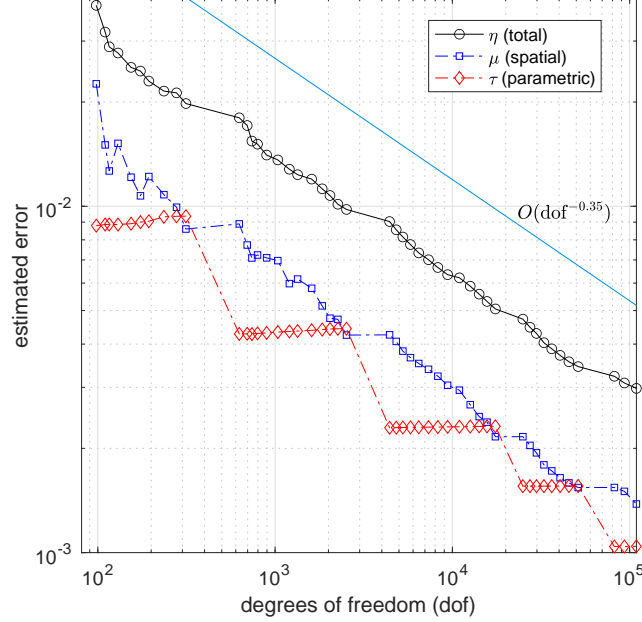


FIGURE 4. Evolution of the error estimates and the error reduction indicators generated by running single-level SG for test case I with error tolerance set to $3\text{e-}3$.

The evolution of the component SG error indicators and the global error estimate is reported in Fig. 4. The total number of iterations is exactly twice the number of adaptive SC steps, with 4 parametric enrichment steps. The parametric approximation space obtained by SG when the error tolerance is satisfied is listed in Table 1 for comparison with SC. The main difference is that there are 5 parameters included in the SG approximation space when the algorithm terminated.² Comparing with adaptive SC the total number of degrees of freedom was reduced by a factor of about 2 (109,152 vs 214,149) as was the overall computation time (29 seconds vs 71 seconds). Reassuringly, the rates of convergence of the SC and SG algorithms can be seen to be closely matched.

The plots in Fig. 5 show the initial mesh together with the mesh when the SG error tolerance is reached. The number of vertices in the final mesh is 7,134. This is less refined than the final mesh in Fig. 2 as might be expected. One obvious difference between the two final meshes is the fact that the mesh generated by adaptive SC has local resolution that captures the distribution of the variance in the reference solution (cf. Fig. 1).

5.2. Test case II: nonaffine coefficient data. In this case, we set $f = 1$ and solve the model problem on the L-shaped domain $D = (-1, 1)^2 \setminus (-1, 0]^2$ with coefficient $a(x, \mathbf{y}) = \exp(h(x, \mathbf{y}))$, where the exponent field $h(x, \mathbf{y})$ has affine dependence on parameters y_m

²The fourth parameter was activated at step 37 and the fifth at step 45.

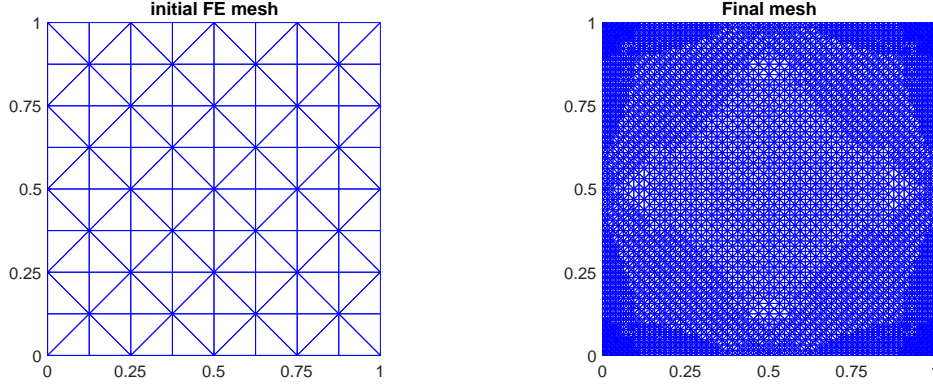


FIGURE 5. The initial mesh (left) and final mesh (right) generated by running single-level adaptive SG for test case I with error tolerance set to $3\text{e-}3$.

that are images of uniformly distributed independent mean-zero random variables,

$$h(x, \mathbf{y}) = h_0(x) + \sum_{m=1}^M h_m(x) y_m, \quad x \in D, \mathbf{y} \in \Gamma. \quad (41)$$

We further specify $h_0(x) = 1$ and $h_m(x) = \sqrt{\lambda_m} \varphi_m(x)$ ($m = 1, \dots, M$). Here $\{(\lambda_m, \varphi_m)\}_{m=1}^\infty$ are the eigenpairs of the integral operator $\int_{D \cup (-1,0]^2} \text{Cov}[h](x, x') \varphi(x') dx'$ with a synthetic covariance function given by

$$\text{Cov}[h](x, x') = \sigma^2 \exp \left(-\frac{|x_1 - x'_1|}{\ell_1} - \frac{|x_2 - x'_2|}{\ell_2} \right), \quad (42)$$

where σ is the standard deviation and ℓ_1, ℓ_2 are correlation lengths (we set $\ell_1 = \ell_2 = 1$). The resulting parametric model problem is uniformly well posed in the sense that (2) is satisfied for any choice of M . If M is fixed then the challenge is to retain robustness when the standard deviation is increased. A test case such as this is more amenable to SC-FEM approximation than the affine test case discussed above. The sparsity of the linear algebra would be severely compromised if this test problem were solved using a stochastic Galerkin approximation strategy; see, e.g., [10].

We present results for three test problems associated with different combinations of the number of parameters M and the standard deviation σ : (a) $M = 4$ and $\sigma = 0.5$, (b) $M = 8$ $\sigma = 0.5$ and (c) $M = 4$ and $\sigma = 1.5$. For all tests we specify the same tolerance ($6\text{e-}3$) and run the algorithm with marking parameters $\theta_{\mathbf{x}} = \theta_{\mathbf{y}} = 0.3$. To assess the effectivity of the error estimation process we also computed a reference solution u_{ref} as a proxy of the exact solution to each problem. The reference solution(s) were generated using the minimum isotropic index set containing the final index set from the adaptive computation together with a piecewise *quadratic* finite element approximation space defined on the final mesh from the adaptive computation.

To measure the quality of the error estimate $\eta_\ell = \mu_\ell + \tau_\ell$ we compute an effectivity index at each iteration via

$$\Theta_\ell = \frac{\eta_\ell}{\|u_{\text{ref}} - u_\ell^{\text{SC}}\|}. \quad (43)$$

Thus, Θ_ℓ being close to 1 suggests that η_ℓ is an effective estimate of the norm of the error.

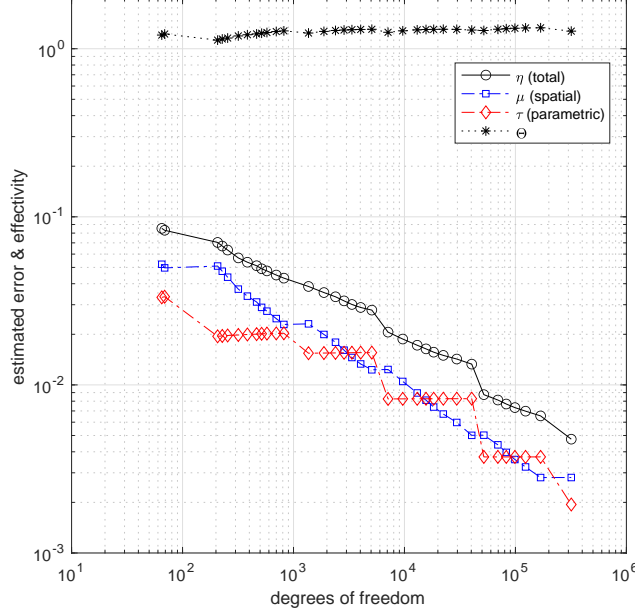


FIGURE 6. Evolution of the error estimates generated by running the single-level adaptive strategy for test case II with $M = 4$ and $\sigma = 0.5$ with the error tolerance set to $6\mathbf{e}-3$.

We record the evolution of the error estimates and the component spatial and parametric contributions together with the effectivity index at each iteration of the single-level adaptive algorithm. Results for the first parameter combination are shown in Fig. 6. The error tolerance was satisfied after 33 iterations which included 5 parametric refinement steps. The plots in Fig. 7 show the initial mesh and the mesh when the error tolerance is reached. The degree of local refinement in the final mesh is strongest around the reentrant corner but is noticeable at all corners of the domain. The number of vertices in the final mesh is 18,737, and there are 17 collocation points in the final sparse grid. The computed effectivity indices plotted in Fig. 6 can be seen to stay close to unity throughout, ranging from a minimum value of 1.125 to a maximum value of 1.333.

Convergence histories for test problems with the other two parameter combinations are presented in Fig. 8 and in Fig. 9. While the number of iteration steps was reduced from 33 to 32 when M was increased from 4 to 8, the number of parametric refinement steps did not change. The number of degrees of freedom at the end is noticeably larger however: this is mainly because the number of vertices in the final mesh has increased by 50% (from 18,737 to 27,651). Reassuringly, the number of collocation points in the final sparse grid has been kept under control, increasing from 15 in \mathbb{R}^4 to 25 in \mathbb{R}^8 . (The reason for this is that the original $M = 4$ sparse grid index set has simply been augmented by extra index entries generating nodes along the axes of the 4 additional coordinate directions. The nodes in the original directions were unchanged.)

The key point that is worth reiterating is the following: while the total error indicator $\bar{\eta}_\ell = \bar{\mu}_\ell + \bar{\tau}_\ell$ is not robust as a measure of the discretization error in cases like this where M is increased, the relative size of the components still seem to provide reliability in the refinement pattern. Moreover, looking at the results in Fig. 8 the effectivity indices can

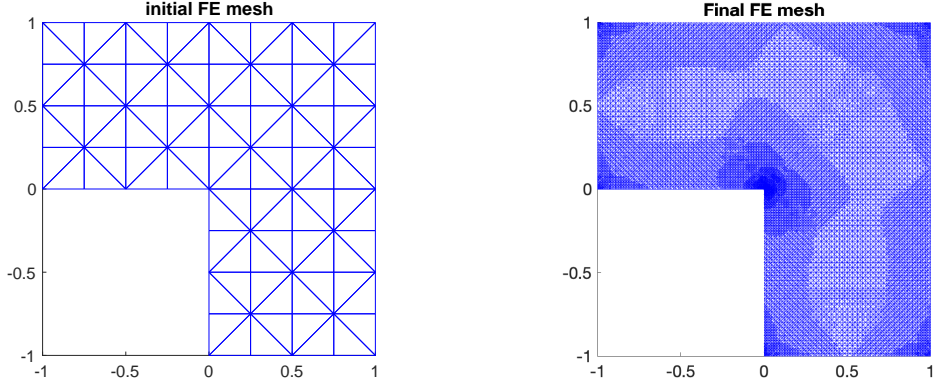


FIGURE 7. The initial mesh (left) and final mesh (right) generated by running the single-level adaptive strategy for test case II with $M = 4$ and $\sigma = 0.5$ with error tolerance set to $6\text{e-}3$.

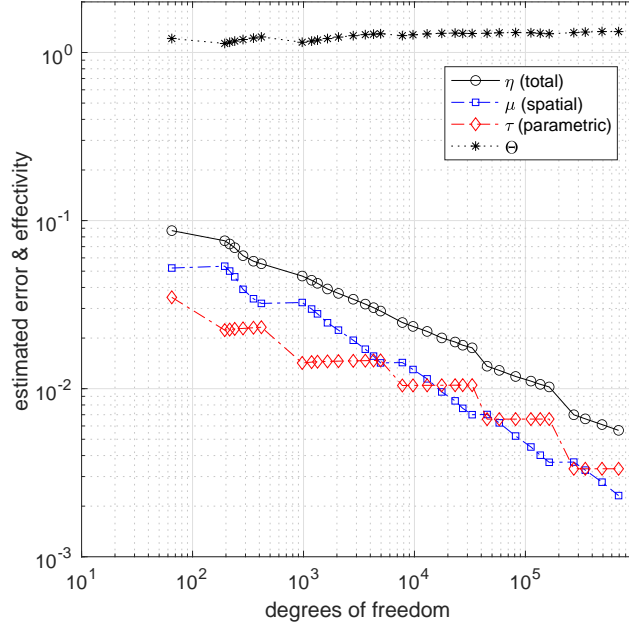


FIGURE 8. Evolution of the error estimates generated by running the single-level adaptive strategy for test case II with $M = 8$ and $\sigma = 0.5$ with the error tolerance set to $6\text{e-}3$.

be seen to stay close to unity throughout the adaptive process, ranging from a minimum value of 1.132 to a maximum value of 1.332. Thus our expectation is that a stopping criterion based on η_ℓ will be reliable in general, not just when M is small.

Turning to the test problem for the third parameter combination, wherein the standard deviation is increased while keeping M fixed, we again see a significant increase in the dimension of the discrete problem at the termination of the adaptive process. While the number of iteration steps is reduced from 33 to 31, the pattern of the refinement is very different in this case. Looking carefully at the convergence history reproduced in Fig. 9, a total of 11 parametric refinement steps can be identified. As a result, the number of

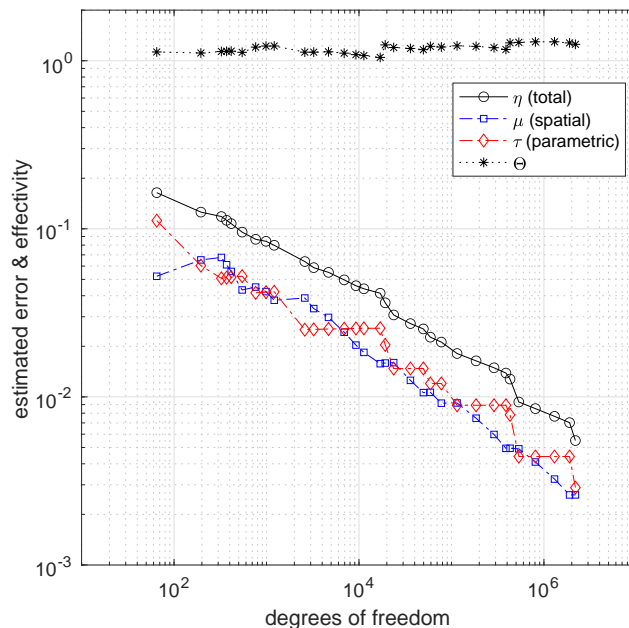


FIGURE 9. Evolution of the error estimates generated by running the single-level adaptive strategy for test case II with $M = 4$ and $\sigma = 1.5$ with the error tolerance set to $6\text{e-}3$.

collocation points in the final sparse grid index set is significantly increased (mirroring the increase in the uncertainty) from 15 when σ is 0.5 to 59 when σ is increased to 1.5. Thus, since the number of vertices in the final mesh has also doubled (going from 18,737 to 37,133) there is an order of magnitude increase in the total number of degrees of freedom needed to solve the test problem to the specified accuracy. The effectivity of the error estimation is also retained, with indices staying between 1.047 and 1.296.

The numerical results presented above demonstrate the effectivity and the robustness of our distinctive SC error estimation strategy as well as the utility of the error indicators guiding the adaptive refinement process. Optimality of convergence is, however, precluded when using the single-level approach. In Part II of this work, we will investigate the realization of close-to-optimal convergence rates within a multilevel framework.

REFERENCES

- [1] M. AINSWORTH AND J. T. ODEN, *A posteriori error estimation in finite element analysis*, Pure and Applied Mathematics (New York), Wiley, 2000.
- [2] I. BABUŠKA, F. NOBILE, AND R. TEMPONE, *A stochastic collocation method for elliptic partial differential equations with random input data*, SIAM J. Numer. Anal., 45 (2007), pp. 1005–1034.
- [3] M. BACHMAYR, A. COHEN, D. DŨNG, AND C. SCHWAB, *Fully discrete approximation of parametric and stochastic elliptic PDEs*, SIAM J. Numer. Anal., 55 (2017), pp. 2151–2186.
- [4] R. B. BANK AND R. K. SMITH, *A posteriori error estimates based on hierarchical bases*, SIAM J. Numer. Anal., 30 (1993), pp. 921–935.
- [5] A. BESPALOV, C. E. POWELL, AND D. SILVESTER, *Energy norm a posteriori error estimation for parametric operator equations*, SIAM J. Sci. Comput., 36 (2014), pp. A339–A363.
- [6] A. BESPALOV, D. PRAETORIUS, L. ROCCHI, AND M. RUGGERI, *Convergence of Adaptive Stochastic Galerkin FEM*, SIAM J. Numer. Anal., 57 (2019), pp. 2359–2382.

- [7] A. BESPALOV AND L. ROCCHI, *Efficient adaptive algorithms for elliptic PDEs with random data*, SIAM/ASA J. Uncertain. Quantif., 6 (2018), pp. 243–272.
- [8] A. BESPALOV, L. ROCCHI, AND D. SILVESTER, *T-IFISS: a toolbox for adaptive FEM computation*, Comput. Math. Appl., (2020). (<https://doi.org/10.1016/j.camwa.2020.03.005>).
- [9] A. BESPALOV AND D. SILVESTER, *Efficient adaptive stochastic Galerkin methods for parametric operator equations*, SIAM J. Sci. Comput., 38 (2016), pp. A2118–A2140.
- [10] A. BESPALOV AND F. XU, *A posteriori error estimation and adaptivity in stochastic Galerkin FEM for parametric elliptic PDEs: beyond the affine case*, Comput. Math. Appl., 80 (2020), pp. 1084–1103.
- [11] A. CHKIFA, A. COHEN, AND C. SCHWAB, *High-dimensional adaptive sparse polynomial interpolation and applications to parametric PDEs*, Found. Comput. Math., 14 (2014), pp. 601–633.
- [12] M. EIGEL, O. G. ERNST, B. SPRUNGK, AND L. TAMELLINI, *On the convergence of adaptive stochastic collocation for elliptic partial differential equations with affine diffusion*, SIAM Journal on Numerical Analysis, 60 (2022), pp. 659–687.
- [13] M. EIGEL, C. J. GITTELSON, C. SCHWAB, AND E. ZANDER, *Adaptive stochastic Galerkin FEM*, Comput. Methods Appl. Mech. Engrg., 270 (2014), pp. 247–269.
- [14] ———, *A convergent adaptive stochastic Galerkin finite element method with quasi-optimal spatial meshes*, ESAIM Math. Model. Numer. Anal., 49 (2015), pp. 1367–1398.
- [15] V. EIJKHOUT AND P. VASSILEVSKI, *The role of the strengthened Cauchy-Buniakowski-Schwarz inequality in multilevel methods*, SIAM Rev., 33 (1991), pp. 405–419.
- [16] M. FEISCHL AND A. SCAGLIONI, *Convergence of adaptive stochastic collocation with finite elements*, Comput. Math. Appl., 98 (2021), pp. 139–156.
- [17] T. GERSTNER AND M. GRIEBEL, *Dimension-adaptive tensor-product quadrature*, Computing, 71 (2003), pp. 65–87.
- [18] D. GUIGNARD AND F. NOBILE, *A posteriori error estimation for the stochastic collocation finite element method*, SIAM J. Numer. Anal., 56 (2018), pp. 3121–3143.
- [19] M. KARKULIK, D. PAVLICEK, AND D. PRAETORIUS, *On 2D newest vertex bisection: Optimality of mesh-closure and H^1 -stability of L_2 -projection*, Constr. Approx., 38 (2013), pp. 213–234.
- [20] J. LANG, R. SCHEICHL, AND D. SILVESTER, *A fully adaptive multilevel stochastic collocation strategy for solving elliptic PDEs with random data*, J. Comput. Phys., 419 (2020), pp. 109692, 17.
- [21] P. MUND AND E. P. STEPHAN, *An adaptive two-level method for the coupling of nonlinear FEM-BEM equations*, SIAM J. Numer. Anal., 36 (1999), pp. 1001–1021.
- [22] P. MUND, E. P. STEPHAN, AND J. WEISSE, *Two-level methods for the single layer potential in \mathbb{R}^3* , Computing, 60 (1998), pp. 243–266.
- [23] F. NOBILE, L. TAMELLINI, AND R. TEMPONE, *Convergence of quasi-optimal sparse-grid approximation of Hilbert-space-valued functions: application to random elliptic PDEs*, Numer. Math., 134 (2016), pp. 343–388.
- [24] F. NOBILE, L. TAMELLINI, F. TESEI, AND R. TEMPONE, *An adaptive sparse grid algorithm for elliptic PDEs with lognormal diffusion coefficient*, in Sparse Grids and Applications—Stuttgart 2014, J. Garcke and D. Pflüger, eds., Springer, 2016, pp. 191–220.
- [25] F. NOBILE, R. TEMPONE, AND C. G. WEBSTER, *A sparse grid stochastic collocation method for partial differential equations with random input data*, SIAM J. Numer. Anal., 46 (2008), pp. 2309–2345.
- [26] S. A. SMOLJAK, *Quadrature and interpolation formulae on tensor products of certain function classes*, Dokl. Akad. Nauk SSSR, 148 (1963), pp. 1042–1045.
- [27] R. STEVENSON, *The completion of locally refined simplicial partitions created by bisection*, Math. Comp., 77 (2008), pp. 227–241.
- [28] A. L. TECKENTRUP, P. JANTSCH, C. WEBSTER, AND M. GUNZBURGER, *A multilevel stochastic collocation method for partial differential equations with random input data*, SIAM/ASA J. Uncertain., 3 (2015), pp. 1046–1074.
- [29] J. ZECH, D. DŨNG, AND C. SCHWAB, *Multilevel approximation of parametric and stochastic PDEs*, Mathematical Models and Methods in Applied Sciences, 29 (2019), pp. 1753–1817.

SCHOOL OF MATHEMATICS, UNIVERSITY OF BIRMINGHAM, EDGBASTON, BIRMINGHAM B15 2TT,
UK

Email address: `a.bespalov@bham.ac.uk`

DEPARTMENT OF MATHEMATICS, UNIVERSITY OF MANCHESTER, OXFORD ROAD, MANCHESTER
M13 9PL, UK

Email address: `d.silvester@manchester.ac.uk`

DEPARTMENT OF MATHEMATICS, UNIVERSITY OF MANCHESTER, OXFORD ROAD, MANCHESTER
M13 9PL, UK

Email address: `feng.xu@manchester.ac.uk`